Journal of Inorganic Biochemistry 194 (2019) 74–84

Contents lists available at ScienceDirect

Journal of Inorganic Biochemistry

journal homepage: www.elsevier.com/locate/jinorgbio

Half-sandwich Ru(η^6-*p*-cymene) complexes featuring pyrazole appended ligands: Synthesis, DNA binding and *in vitro* cytotoxicity

Yen-Chung Huang[a,1], Jebiti Haribabu[a,b,1], Ching-Ming Chien[c,d], Gopal Sabapathi[e], Chon-Kit Chou[c], Ramasamy Karvembu[b], Ponnambalam Venuvanalingam[e], Wei-Min Ching[f], Ming-Li Tsai[g], Sodio C.N. Hsu[a,g,h,*]

[a] Department of Medicinal and Applied Chemistry, Kaohsiung Medical University, Kaohsiung 807, Taiwan
[b] Department of Chemistry, National Institute of Technology, Tiruchirappalli 620 015, India
[c] Department of Biotechnology, Kaohsiung Medical University, Kaohsiung 807, Taiwan
[d] Institute of Genomics and Bioinformatics, National Chung Hsing University, Taichung 402, Taiwan
[e] Theoretical and Computational Chemistry Laboratory, School of Chemistry, Bharathidasan University, Tiruchirappalli 620024, India
[f] Instrumentation Center, Department of Chemistry, National Taiwan Normal University, Taipei 11677, Taiwan
[g] Department of Chemistry, National Sun Yat-Sen University, Kaohsiung 804, Taiwan
[h] Department of Medical Research, Kaohsiung Medical University Hospital, Kaohsiung 807, Taiwan

A B S T R A C T

Organometallic Ru(II)-arene complexes have emerged as potential alternatives to platinum appended agents due to their wide range of interesting features such as stability in solution and solid, significant activity, less toxicity and hydrophobic property of arene moiety, *etc.* Hence, a series of Ru(II)-*p*-cymene complexes, [(η^6-*p*-cymene)Ru(η^2-*N,N*-L1)Cl]Cl (**1**), [(η^6-*p*-cymene)Ru(η^1-*N*-L2)Cl_2] (**2**) and [(η^6-*p*-cymene)Ru(η^1-*N*-L3)Cl_2] (**3**) were prepared from pyrazole based ligands [2-(1H-pyrazol-3-yl)pyridine (L1), 3-(furan-2-yl)-1H-pyrazole (L2) and 3-(thiophen-2-yl)-1H-pyrazole (L3)], and [$RuCl_2$-(η^6-*p*-cymene)] dimer. The new Ru(II)-*p*-cymene complexes were well characterized by elemental analysis, and spectroscopic (FT-IR, UV–Visible, ^{1}H NMR, ^{13}C NMR and mass) and crystallographic methods. The Ru(II)-*p*-cymene complexes (**1**–**3**) were found to adopt their characteristic piano stool geometry around Ru(II) ion. The calf thymus DNA (CT-DNA) binding ability of the new complexes was investigated by electronic absorption spectroscopic titration and viscosity methods. The molecular docking study results showed that complex **1** strongly bound with targeted biomolecules than **2** and **3**. Docked poses of bidentate pyrazole based Ru(II)-*p*-cymene complex **1** revealed that the complex formed a crucial guanine N^7 position hydrogen bond with DNA receptor. Complexes **1**–**3** might hydrolyze under physiological conditions and form aqua complexes **4**–**8**, and docking calculations showed that the aqua complexes bound strongly with the receptors than original complexes. The *in vitro* cytotoxicity of the Ru(II)-*p*-cymene complexes and cisplatin was evaluated against triple negative breast cancer (TNBC) MDA-MB-231 cells. Our results showed that the inhibitory effect of bidentate pyrazole based Ru(II)-*p*-cymene complex **1** on the growth of breast cancer cells was superior to other tested complexes.

1. Introduction

Complexes of transition metals have, over the decades, significantly contributed in various aspects to the field of pharmaceutical chemistry, after the establishment of cisplatin as an anticancer drug late in 1975 [1–4]. The organometallic complexes over the years have shown numerous beneficial properties marking them as chemotherapeutic agents [5]. Drugs having electron deficient metal centres are known to target the electron rich biomolecules either by covalent or non-covalent interactions. The target of these complexes can be the DNA, an enzyme, a cell surface receptor, nuclear hormone receptor, ion channel or a transporter [6,7].

The current scenario has a great number of scientists exploring the coordination chemistry of chelated ligands with mixed functionalities on transition metal centres [8]. A subset of this, transition metal complexes containing arene as a coordinated group, which is a π-bonded ligand, have gained attention from the viewpoints of improving and elucidating the properties of complexes. In particular, the piano stool three-legged ruthenium(II)-arene complexes have grown in popularity in recent years due to their positive establishment in both catalytic and pharmaceutical industries [9–18]. A couple of ruthenium complexes namely NAMI-A and KP1019 have already entered phase II of clinical trials which stress the importance of ruthenium as a biologically active metal centre [19].

Complexes of the type [M(arene)Cl_2]$_2$ (arene = benzene, cymene, toluene, biphenyl, *etc.*) have been used progressively in medicinal

* Corresponding author at: Department of Medicinal and Applied Chemistry, Kaohsiung Medical University, Kaohsiung 807, Taiwan.
E-mail address: sodiohsu@kmu.edu.tw (S.C.N. Hsu).
[1] Both the authors contributed equally to this work.

https://doi.org/10.1016/j.jinorgbio.2019.02.012
Received 5 November 2018; Received in revised form 11 February 2019; Accepted 18 February 2019
Available online 23 February 2019
0162-0134/

inorganic chemistry as precursors for the preparation of different potential metallodrugs with promising activities, for example, against cancer, immunodeficiency virus (HIV), bacteria and parasites [20–26]. The chemical and physical properties of such complexes can be tuned successfully by varying the ligands present on the "legs" of the piano-stool complexes. The chloride ligands are susceptible to substitution and can be easily replaced by stronger donor molecules [27,28]. Ruthenium(II) complexes of the type [Ru(X)(η^6-arene)L)] (where L is a bidentate or two monodentate ligands and X is a leaving group, *e.g.* Cl^-) showed significant *in vitro* and *in vivo* anticancer properties; some cases are even comparable with cisplatin [17]. The aqueous reactivity of [Ru(X)(η^6-arene)L)] complexes is highly dependent on the nature of X, L, and the arene moiety. Complexes of the type [(η^6-arene)Ru(ethylenediamine)Cl]$^+$ displayed cytotoxic activity both *in vitro* and *in vivo*, against cisplatin-resistant cancer cells [29]. Particularly, the Ru(II)-arene complexes bearing nitrogen donor ligands exhibited good biological activities [7,20,30–33].

Over the time, since the development of coordination chemistry, various new chelating *N* heterocyclic ligands have been synthesized. A family of nitrogen containing pyrazole and thiazole based ligands has particularly been widely studied and offered a diversity of applications [34]. There have been reports on pyrimidyl pyrazole derivatives being used as antitumor agents and shown antiproliferative effect on human lung cancer cell line as well as inhibited the polymerization of tubulin. The most probable way in which pyrazole based compounds exhibit bioactivity is by the formation of hydrogen bond with biomolecules [7,35,36]. Organometallic complexes containing such ligands are considered as potential DNA intercalators with the capability to inhibit synthesis of nucleic acid. These ligands are also known to have varying properties such as catalytic, redox and photoredox with divergent metal precursors particularly with ruthenium [37–40]. When the strong σ-donor ability of pyrazole group and π-accepting property of pyridyl ring are joined together, it may give rise to properties different from those of the isolated moieties.

The biological uses of ruthenium(II)-arene complexes and pyrazole-based ligands [2-(1H-pyrazol-3-yl)pyridine (L1), 3-(furan-2-yl)-1H-pyrazole (L2) and 3-(thiophen-2-yl)-1H-pyrazole (L3)] have motivated us to design three Ru(II)-*p*-cymene complexes with the formula [(η^6-*p*-cymene)Ru(η^2-*N,N*-L1)Cl]Cl (**1**), [(η^6-*p*-cymene)Ru(η^1-*N*-L2)Cl_2] (**2**) and [(η^6-*p*-cymene)Ru(η^1-*N*-L3)Cl_2] (**3**). The complexes were well characterized using analytical and spectroscopic methods. The exact molecular structure of all the complexes was determined by single crystal X-ray diffraction technique. The biological properties like DNA binding and *in vitro* anticancer activity are also reported in this paper.

2. Experimental section

2.1. Materials and methods

[$RuCl_2$(η^6-*p*-cymene)]$_2$ was synthesized by following a literature method [41]. 2-(1H-pyrazol-3-yl)pyridine (L1), 3-(furan-2-yl)-1H-pyrazole (L2) and 3-(thiophen-2-yl)-1H-pyrazole (L3) ligands were synthesized by using a previously reported method [42–44]. Complex **3** was synthesized according to previously reported method with slight modification in the procedure [7]. UV–Visible spectra were acquired on an Agilent 8453 spectrophotometer. IR spectra were recorded on a Varian FT-IR 640 spectrometer. Elemental analyses were performed on a Heraeus CHN-OS rapid elemental analyzer. NMR spectra were collected on a Varian Gemini-400 proton/carbon FT-NMR spectrometer. ESI-MS spectra were performed using a Waters ZQ 4000 mass spectrometer.

2.2. Synthetic procedure of Ru(II)-p-cymene complexes 1-3

To a methanolic (5 mL) solution of pyrazole based ligand (L1-L3, 134–150 mg, 1 mmol), was added a methanolic (5 mL) solution of [$RuCl_2$(η^6-*p*-cymene)]$_2$ (30.6 mg, 0.5 mmol), and the reaction mixture was allowed to stir for 4 h at room temperature. The solution was concentrated to 3 mL under reduced pressure, and addition of petroleum ether (10–12 mL) gave a clear orange/yellowish orange solid. The solid was collected by filtration, washed with petroleum ether many times and air dried. The complexes were recrystallized from chloroform-acetonitrile mixture.

2.3. [(η^6-p-cymene)Ru(η^2-N,N-L1)Cl]Cl (1)

2-(1H-pyrazol-3-yl)pyridine ligand (L1, 145 mg, 1 mmol) was utilized. Yield: 90%. Color: Orange solid. UV–Vis (CH_3OH): λ_{max}, nm (ε, $dm^3\,mol^{-1}\,cm^{-1}$) 421 (1000), 324 (4500), 290 (8700). FT-IR (KBr): ν, cm^{-1} 3402 (N—H), 1613 (C=C), 1433 (C=N). ^{1}H NMR (400 MHz, DMSO-d_6): δ, ppm 15.73 (s, 1H, NH), 9.43 (dd, *J* = 4.6, 0.9 Hz, 1H, aromatic-H), 8.31 (d, *J* = 2.8 Hz, 1H, aromatic-H), 8.24–8.12 (m, 2H, aromatic-H), 7.60 (ddd, *J* = 7.3, 5.7, 1.8 Hz, 1H, aromatic-H), 7.26 (d, *J* = 2.8 Hz, 1H, aromatic-H), 6.38 (d, *J* = 6.1 Hz, 1H, *p*-cymene aromatic-H), 6.16 (d, *J* = 6.1 Hz, 1H, *p*-cymene aromatic-H), 6.07 (d, *J* = 6.1 Hz, 1H, *p*-cymene aromatic-H), 5.95 (d, *J* = 6.1 Hz, 1H, *p*-cymene aromatic-H), 2.62–2.52 (m, 1H, *p*-cymene C**H**(CH_3)$_2$), 2.18 (s, 3H, *p*-cymene CH_3), 0.90 (dd, *J* = 6.6, 2.9 Hz, 6H, *p*-cymene CH(C**H$_3$**)$_2$). ^{13}C NMR (100 MHz, DMSO-d_6): δ, ppm 155.45, 150.31 (C=N), 149.50, 139.76, 135.22, 125.04, 122.13, 104.34 (aromatic carbons), 103.07, 102.77, 85.00, 83.91, 83.01, 81.56 (aromatic carbons of *p*-cymene), 30.41, 21.70, 21.44, 18.45 (aliphatic carbons of *p*-cymene). ESI$^+$: *m/z* Found (Calcd.) 415.94 (416.05) [M-Cl]$^+$. Anal. Calc. $C_{18}H_{21}Cl_2N_3Ru{\cdot}0.5H_2O$ (%): C, 46.96; H, 4.82; N, 9.13. Found: C, 46.78; H, 4.91; N, 9.00. Mp (°C): 258.

2.4. [(η^6-p-cymene)Ru(η^1-N-L2)Cl_2] (2)

3-(furan-2-yl)-1H-pyrazole (L2, 134 mg, 1 mmol) was utilized. Yield: 40%. Color: Yellowish orange solid. UV–Vis (CH_3OH): λ_{max}, nm (ε, $dm^3\,mol^{-1}\,cm^{-1}$) 434 (600), 324 (1200), 272 (19400). FT-IR (KBr): ν, cm^{-1} 3459 (N—H), 1627 (C=C), 1413 (C=N). ^{1}H NMR (400 MHz, DMSO-d_6): δ, ppm 12.94 (s, 1H, NH), 7.78–7.52 (m, 2H, aromatic-H), 6.69–6.55 (m, 2H, aromatic-H), 6.51 (d, *J* = 2.6 Hz, 1H), 5.82 (d, *J* = 6.4 Hz, 2H, *p*-cymene aromatic-H), 5.78 (d, *J* = 6.4 Hz, 2H, *p*-cymene aromatic-H), 2.99–2.66 (m, 1H, *p*-cymene C**H**(CH_3)$_2$), 2.08 (s, 3H, *p*-cymene CH_3), 1.19 (d, *J* = 6.9 Hz, 6H, *p*-cymene CH(C**H$_3$**)$_2$). ^{13}C NMR (100 MHz, DMSO-d_6): δ, ppm 141.87 (C=N), 129.48, 111.44, 106.32, 105.04 (aromatic carbons), 101.57, 100.06, 86.34, 85.49 (aromatic carbons of *p*-cymene), 29.96, 21.48, 17.86 (aliphatic carbons of *p*-cymene). ESI$^+$: *m/z* Found (Calcd.) 405.07 (405.03) [M-Cl]$^+$. Anal. Calc. $C_{17}H_{20}Cl_2N_2ORu$ (%): C, 46.37; H, 4.58; N, 6.36. Found: C, 45.46; H, 4.76; N, 6.19. Mp (°C): 185.

2.5. [(η^6-p-cymene)Ru(η^1-N-L3)Cl_2] (3)

3-(thiophen-2-yl)-1H-pyrazole (L3, 150 mg, 1 mmol) was utilized. Yield: 50%. Color: Yellowish orange solid. UV–Vis (CH_3OH): λ_{max}, nm (ε, $dm^3\,mol^{-1}\,cm^{-1}$) 419 (570), 331 (3000), 274 (6800). FT-IR (KBr): ν, cm^{-1} 3463 (N—H), 1627 (C=C), 1413 (C=N). ^{1}H NMR (400 MHz, DMSO-d_6): δ, ppm 12.83 (s, 1H, NH), 7.76–7.74 (m, 1H, aromatic-H), 7.39 (dd, *J* = 15.5, 3.7 Hz, 2H, aromatic-H), 7.10–7.03 (m, 1H, aromatic-H), 6.59 (d, *J* = 2.9 Hz, aromatic-H), 5.82 (d, *J* = 6.4 Hz, 2H, *p*-cymene aromatic-H), 5.78 (d, *J* = 6.4 Hz, 2H, *p*-cymene aromatic-H), 2.88–2.78 (m, 1H, *p*-cymene C**H**(CH_3)$_2$), 2.08 (s, 3H, *p*-cymene CH_3), 1.19 (d, *J* = 6.9 Hz, 6H, *p*-cymene CH(C**H$_3$**)$_2$). ^{13}C NMR (100 MHz, DMSO-d_6): δ, ppm 145.62 (C=N), 129.93, 127.51, 124.37, 123.43, 106.32 (aromatic carbons), 101.63, 100.05, 86.34, 85.49 (aromatic carbons of *p*-cymene), 29.96, 21.48, 17.86 (aliphatic carbons of *p*-cymene). ESI$^+$: *m/z* Found (Calcd.) 420.85 (421.01) [M-Cl + CH_3CN]$^+$. Anal. Calc. $C_{17}H_{20}Cl_2N_2SRu$ (%): C, 44.74; H, 4.42; N, 6.14; S, 7.02. Found: C, 44.72; H, 4.48; N, 6.34; S, 7.14. Mp (°C): 197.

2.6. X-ray crystal structure determinations

Suitable crystals of complexes **1**, **2**, and **3** were obtained from slow evaporation of methanol solution of the samples. Single crystal X-ray diffraction data were collected using a Bruker Nonius Kappa CCD diffractometer with Mo*K*α radiation (λ = 0.71073 A). The Bruker SMART program package was used to determine the unit cell parameters and collect the data. All the structures were solved by direct methods and were refined on F^2 by the full-matrix least-squares method using the SHELXL-2014 program [45]. All the non-hydrogen atoms were refined anisotropically, whereas hydrogen atoms were placed at the calculated positions and were included in the final stage of refinements with fixed parameters. Further details are given in Table S1 in the Supporting Information.

2.7. DNA binding experiments

The experiments were carried out in 50 mM NaCl/5 mM Tris HCl (pH 7.2) solution at ambient temperature. The purity of calf thymus DNA (CT-DNA) was verified by taking the ratio of the absorbance values at 260 and 280 nm in the respective buffer, which was found to be 1.9:1, indicating the absence of any protein impurities in the DNA sample. The molar absorption coefficient of CT-DNA (6600 M^{-1} cm^{-1}) at 260 nm was used to find out the CT-DNA concentration. Stock solutions were stored at 4 °C and used within 4 days. Absorption titration experiments were made using different concentrations of CT-DNA, while keeping the complex concentration as constant. Samples were equilibrated before recording each spectrum [46,47]. The concentration of the complexes used was 20 μM; CT-DNA of varying concentration (0–35 μM) was added each time, and the significant absorbance change was noted.

2.8. Viscosity measurements

Viscosity experiments were carried out using a semi-micro viscometer maintained at 27 °C in a thermostatic water bath. Flow time of solutions in Tris-HCl buffer (pH 7.2) was recorded in triplicate for each sample, and an average flow time was calculated from the digital timer attached with the viscometer. For viscosity measurements, CT-DNA concentration was kept constant (100 μM) and the concentration of the complexes varied (1/R = [Complex]/[DNA]). Data are presented as η/η^0 *versus* 1/R, where η is the relative viscosity of DNA in the presence of complex (0–60 μM), and η^0 is the relative viscosity of DNA alone. Relative viscosity values were calculated from the observed flow time of the DNA solution (t) corrected for the flow time of the buffer alone (t^0), using the expression $\eta^0 = (t\text{-}t^0)/t^0$ [48].

2.9. Computational details

Initial geometries of complexes **1–3** were retrieved from the X-ray crystal structures, while those of corresponding aqua complexes [(η^6-*p*-cymene)Ru(η^2-*N,N*-L1)(OH_2)]$^{2+}$ (**4**), [(η^6-*p*-cymene)Ru(η^1-*N*-L2)(OH_2)Cl]$^+$ (**5**), [(η^6-*p*-cymene)Ru(η^1-*N*-L2)$(OH_2)_2$]$^{2+}$ (**6**), [(η^6-*p*-cymene)Ru(η^1-*N*-L3)(OH_2)Cl]$^+$ (**7**), and [(η^6-*p*-cymene)Ru(η^1-*N*-L3)$(OH_2)_2$]$^{2+}$ (**8**) were obtained by progressively replacing the chloride ligand by water molecules in the original complexes and the optimized structures of these complexes **1–8** are presented in Fig. 7. The ground state geometry of the Ru(η^6-*p*-cymene) complexes was fully optimized using density functional theory (DFT) with the B3LYP [49,50] functional and SDD basis set (for Ru)/6-311 g(d,p) basis set (for H, C, N, O, S and Cl atoms). Geometry optimizations were performed without any symmetry constraints with methanol as solvent using the polarizable continuum model (PCM) using Gaussian 09 [51]. Harmonic analysis was performed to confirm that the optimized structures were local minima. The coordinates of the Ru(η^6-*p*-cymene) complexes obtained from optimized geometries were converted into .pdb format using GaussView 5.0.9 software [52]. The high resolution crystal structures of human B-DNA (PDB ID: 1BNA) and human DNA topoisomerase I (PDB ID: 1SC7) were obtained from the protein data bank (http://www.rcsb.org/pdb). All the water molecules, and heteroatoms were removed from the B-DNA and topoisomerase I. Before performing docking calculations, receptor was refined by minimization and optimization using the OPLS3 force field. Docking calculations were performed using the DFT optimized Ru(II)-*p*-cymene complexes **1–8** with B-DNA and topoisomerase I, using Glide (Glide, version 6.8, Schrödinger, LLC, New York, NY, 2015) by means of XP precision mode and its output Glide score was calculated [53–55]. Finally, visualization and analysis of the docked systems have been done using Discovery Studio 4.0 Client and PyMOL software packages [56].

2.10. Cell culture

The triple negative breast cancer (TNBC) MDA-MB-231 (ATCC® HTB-26™) and human normal bronchial epithelium cells BEAS-2B (ATCC® CRL-9609™) were obtained from the American Type Culture Collection (ATCC; Manassas, VA, USA). The tested cells were maintained in DMEM (Dulbecco's modified eagle's medium)/F12 (3:2) supplemented with 8% FBS (fetal bovine serum), 2 mM glutamine, and antibiotics (100 units/mL penicillin and 100 μg/mL streptomycin) at 37 °C in a humidified atmosphere of 5% CO_2.

2.11. Cell proliferation assay

Cytotoxicity of **1–3**, and cisplatin was studied by using the MTS [3-(4,5-dimethylthiazol-2-yl)-5-(3-carboxymethoxyphenyl)-2-(4-sulfophenyl)-2H-tetrazolium] assay [57]. All the cell lines were cultured and maintained in DMEM containing 10% FBS along with antibiotics (penicillin and streptomycin). The 5 × 10^3 cells/well were seeded in a 96-well plate and incubated with the humidified condition at 37 °C with 5% CO_2. The cells were treated with different concentrations of the complexes (0–100 μM) and incubated for 24 h. After treatment, the cells were washed twice with PBS and incubated with diluted fresh MTS media for 4 h. The data were taken at 490 nm. By using the formula A-B /A × 100 (A = control group and B = treated group), inhibition (%) was calculated. Each point represents the mean ± SD of three replicates.

2.11.1. Statistical analysis

Statistical analysis was performed by student's *t*-test for cell assays. * represents $p < 0.05$ and ** represents $p < 0.01$, which was considered significant.

3. Results and discussion

3.1. Synthesis and spectroscopic analyses of the complexes

The pyrazole-based ligands (L1 − L3) were prepared using the reported procedure [42–44]. The complexes [(η^6-*p*-cymene)Ru(η^2-*N,N*-L1)Cl]Cl (**1**), [(η^6-*p*-cymene)Ru(η^1-*N*-L2)Cl_2] (**2**), and [(η^6-*p*-cymene)Ru(η^1-*N*-L3)Cl_2] (**3**) were synthesized from pyrazole-based ligands (L1-L3) and [$RuCl_2(\eta^6$-*p*-cymene)$]_2$ precursor in 2:1 M ratio in methanol at room temperature (Scheme 1). With L1, reaction took place through chloro-bridge cleavage, followed by dissociation of one chloride from the starting material to give an ionic complex **1** with bidentate ligand and one chloride as a counter ion. L2 and L3 coordinated to Ru ion as monodentate ligand to form neutral complexes **2** and **3**, respectively. Complex **3** was reported in a publication [7] that appeared during the preparation of the current manuscript. All the complexes are yellow-orange crystalline solid, air and light stable, non-hygroscopic, and highly soluble in methanol, acetone, acetonitrile, dimethylsulfoxide, dimethylformamide, and H_2O. Complexes **2** and **3** are also soluble in dichloromethane and chloroform. In addition, all the complexes **1–3**

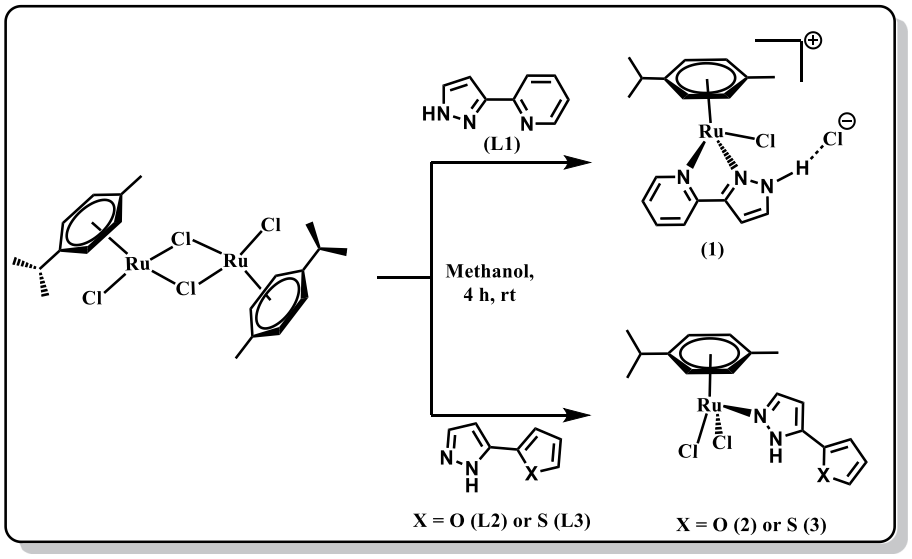

Scheme 1. Synthesis of bidentate and monodentate Ru(II)-*p*-cymene complexes.

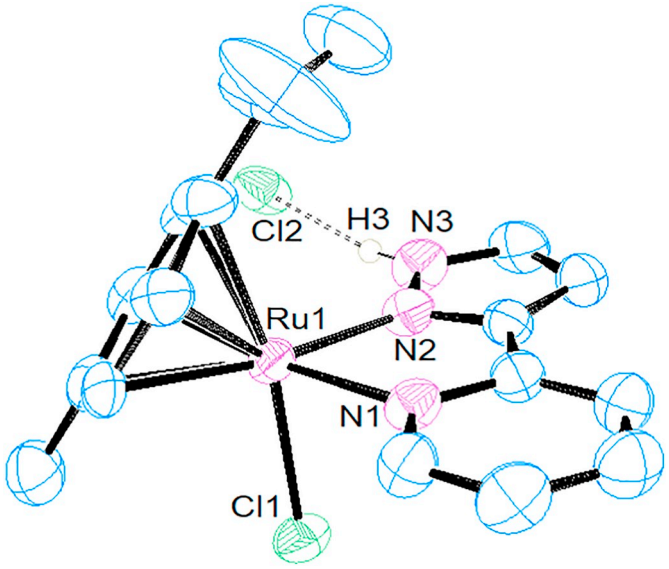

Fig. 1. Thermal ellipsoidal plot of **1** at 50% probability level. Hydrogen atoms are not shown for clarity. Selected bond distances (Å) and angles (°): Cl(1)-Ru (1) 2.3973(12), N(1)-Ru(1) 2.120(4), N(2)-Ru(1) 2.090(4), N(3)-N(2)-Ru(1) 134.8(3), N(2)-Ru(1)-N(1) 75.40(15), N(2)-Ru(1)-Cl(1) 87.56(11), N(1)-Ru(1)-Cl(1) 83.51(11).

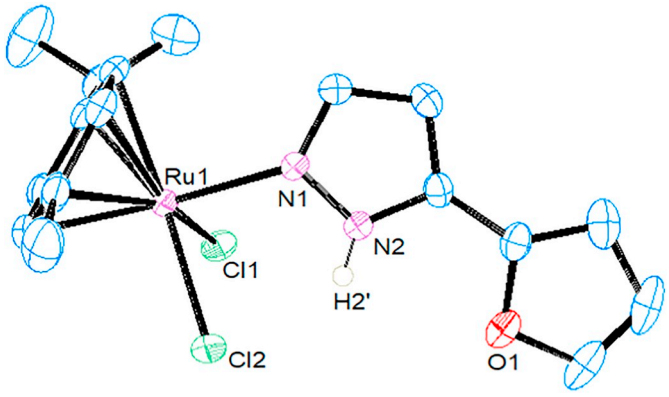

Fig. 2. Thermal ellipsoidal plot of **2** at 50% probability level. Hydrogen atoms are not shown for clarity. Selected bond distances (Å) and angles (°): Cl(1)-Ru (1) 2.4110(6), Cl(2)-Ru(1) 2.4387(5), N(1)-Ru(1) 2.1085(17), N(2)-N(1)-Ru(1) 119.95(12), N(1)-Ru(1)-Cl(1) 83.74(5), N(1)-Ru(1)-Cl(2) 85.08(5), Cl(1)-Ru(1)-Cl(2) 87.457(19).

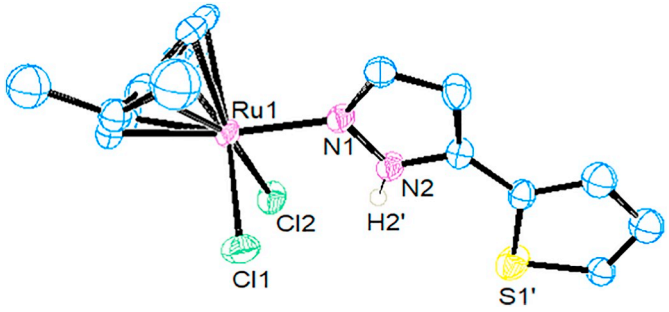

Fig. 3. Thermal ellipsoidal plot of **3** at 50% probability level. Hydrogen atoms are not shown for clarity. Selected bond distances (Å) and angles (°): Cl(1)-Ru (1) 2.4057(13), Cl(2)-Ru(1) 2.4384(12), N(1)-Ru(1) 2.107(4), N(2)-N(1)-Ru(1) 120.6(3), N(1)-Ru(1)-Cl(1) 83.38(11), N(1)-Ru(1)-Cl(2) 85.49(10), Cl(1)-Ru(1)-Cl(2) 87.21(5).

were characterized by elemental analyses and FT-IR, NMR, ESI-MS, and UV–Visible spectroscopy. Finally, coordination mode of the ligands and geometry of the complexes were determined by single crystal X-ray analysis.

UV–Visible spectra of complexes **1–3** contained intra-ligand ($\pi \rightarrow \pi^*$ and $n \rightarrow \pi^*$) and $d \rightarrow d$ transition bands at 272–331 and 419–434 nm respectively [31,58]. IR spectra of the complexes contained C═N (**1**, **2** and **3**) stretching band at 1413–1433 cm^{-1} which was lower than that of free pyrazole ligand, indicating the coordination of nitrogen to Ru(II) ion. The broad band in the range 3402–3463 cm^{-1} might be due to the stretching of N—H bond.

NMR spectra of all the complexes were recorded in DMSO-d_6. The N—H signal was shown in the downfield at 15.73 ppm in the spectrum of complex **1** due to stronger hydrogen bonding between pyrazole NH and uncoordinated Cl. The same proton in complexes **2** and **3** appeared at 12.94 and 12.83 ppm respectively. The aromatic protons of *p*-cymene moiety were shielded and gave four doublets at 6.38, 6.16, 6.07 and 5.95 ppm in the spectrum of complex **1**, whereas in the spectra of complexes **2** and **3**, these protons were observed as two doublets at 5.82 and 5.78 ppm [59]. The isopropyl CH, methyl, and isopropyl methyl protons were also shielded and observed in the regions 2.62–2.52,

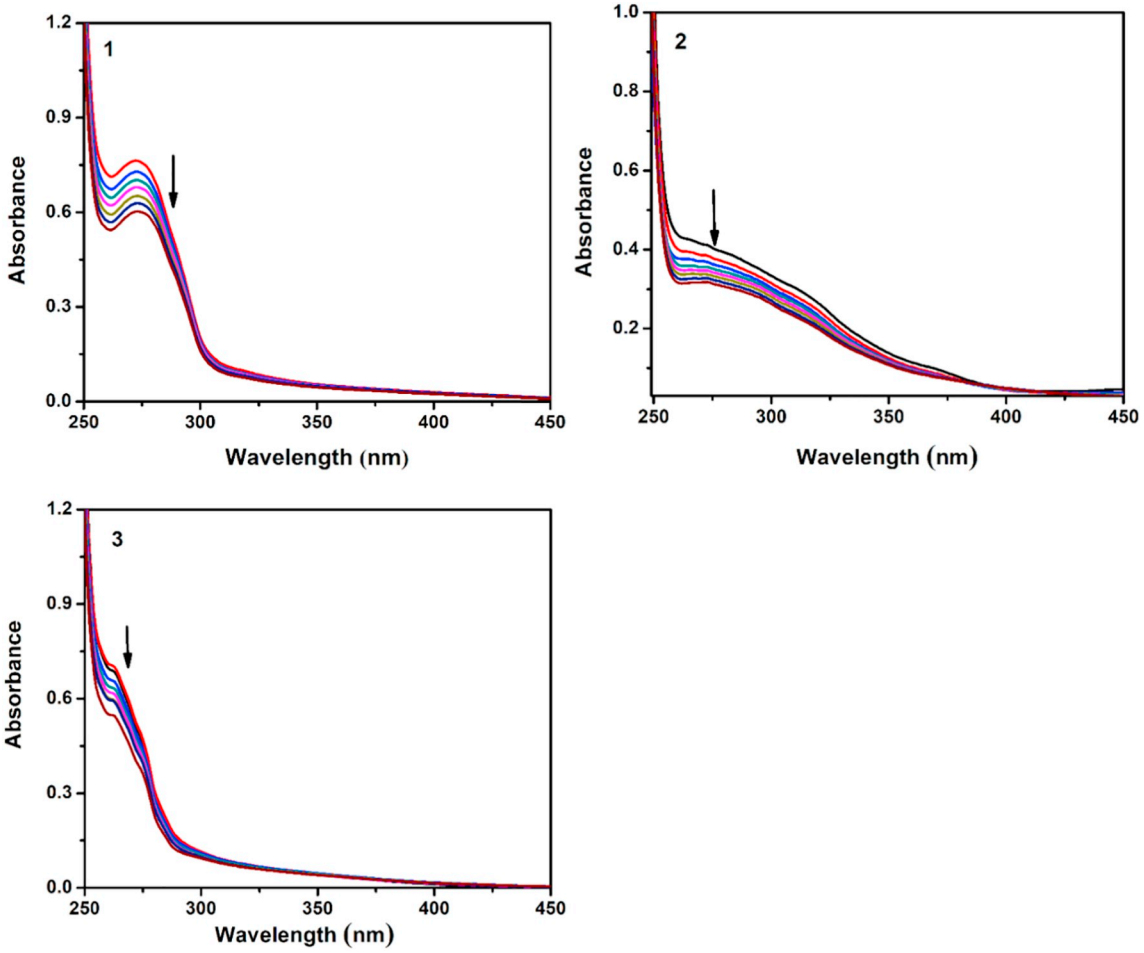

Fig. 4. Absorption spectra of complexes **1**, **2** and **3** in Tris-HCl buffer upon addition of CT DNA. [Complex] = 2.0×10^{-5} M, [DNA] = 0–35 μM. The arrow shows that the absorption intensities decrease upon increasing DNA concentration.

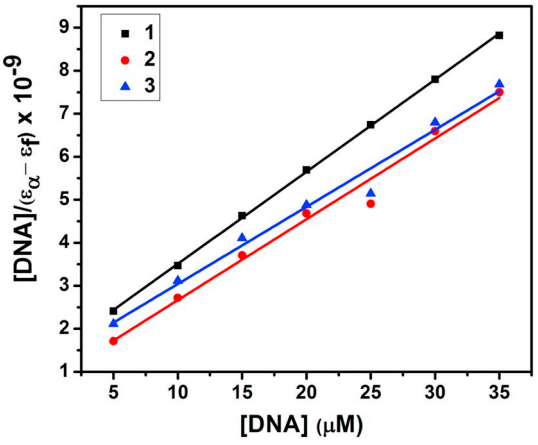

Fig. 5. Plot of [DNA]/(ε_a-ε_f) *versus* [DNA] for the titration of the complexes with CT DNA.

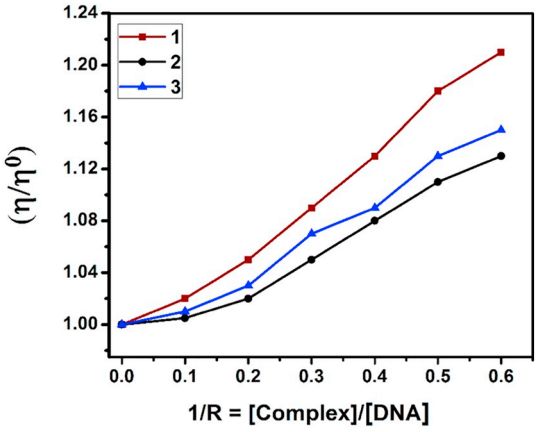

Fig. 6. Effect of complexes **1–3** on the viscosity of CT DNA.

2.99–2.66 and 2.88–2.78 ppm, respectively. In the ^{13}C NMR spectra of the complexes, the signals appeared around 101.63–101.57, 100.06–100.05, 86.34, 85.49 ppm were assigned to aromatic carbons of *p*-cymene group. The isopropyl CH, methyl and isopropyl methyl carbons in *p*-cymene moiety were observed at 29.96, 21.48 and 17.86 ppm, respectively. These new proton and carbon signals indicated formation of the complexes [60]. All other protons and carbons were located in the expected regions.

3.2. X-ray structures

The molecular structures of all the complexes (**1**, **2**, and **3**) were ascertained by single crystal X-ray diffraction analysis, and crystal structures are displayed in Figs. 1–3. The complexes crystallized in orthorhombic (**1**) and monoclinic (**2** and **3**) crystal systems with *Pbca* and $P2_1/n$ space group respectively. Three-dimensional molecular structures of the complexes confirmed the bidentate (η^2-*N,N*, **1**) and monodentate (η^1-*N*, **2** and **3**) coordination mode of the pyrazole-based ligands. In complexes **1–3**, Ru(II) ion adopted half-sandwich "three-

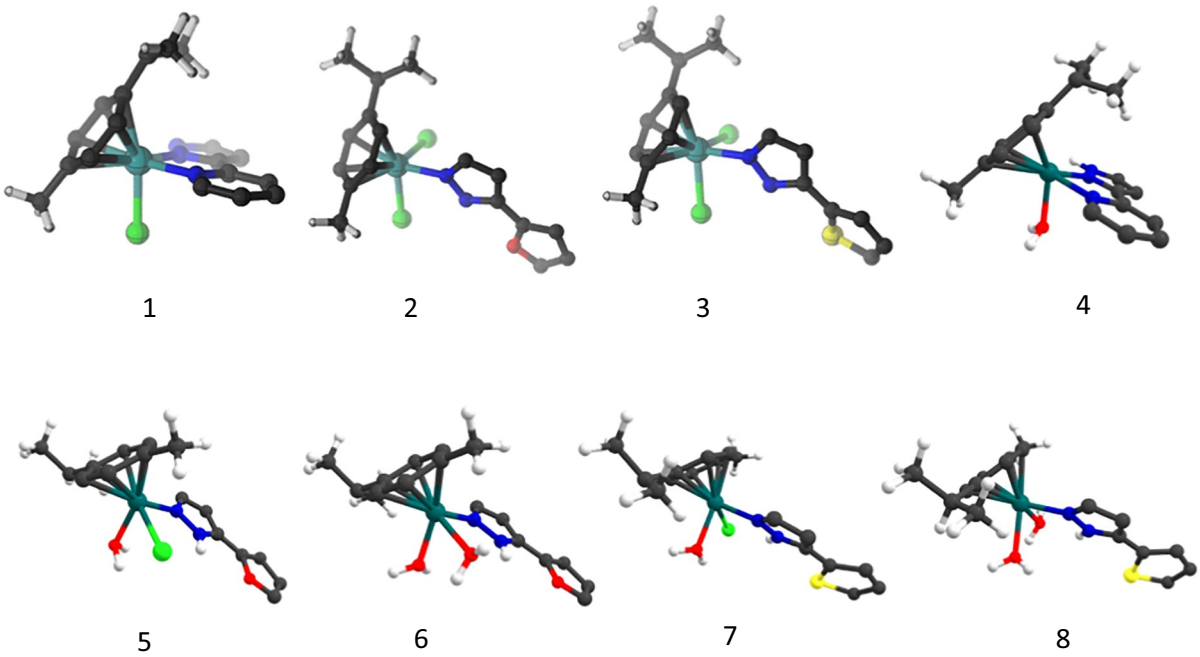

Fig. 7. Optimized geometries of Ru(II)-*p*-cymene complexes **1–3** and their corresponding aqua complexes **4–8**.

Table 1
Selected experimental and computed bond lengths (Å) and bond angles (°) of the optimized Ru^{II} complexes.

	Experimental			Calculated*		
	1	**2**	**3**	**1**	**2**	**3**
Ru-Centroid	2.202	2.179	2.229	2.253	2.229	2.229
Ru(1)-N1	2.120	2.108	2.107	2.140	2.145	2.143
Ru(1)-Cl	2.397	2.411	2.405	2.448	2.477	2.494
Ru(1)-Cl2	–	2.438	2.438	–	2.492	2.477
Ru(1)-N2	2.090	–	–	2.092	–	–
N(1)-Ru(1)-Cl(1)	83.5	83.7	85.4	84.5	84.6	86.3
N(1)-Ru(1)-Cl(2)	–	85.0	83.3	–	86.4	84.5
Cl(1)-Ru(1)-Cl(2)	–	87.4	87.2	–	86.8	86.6

*Calculated at B3LYP/SDD# (#SDD (Ru), 6-311 g (d, p) for other atoms) level.

legged piano-stool" geometry, the η^6-*p*-cymene occupied the "seat of the stool", one chloride (**1**) or two chlorides (**2** and **3**) and two nitrogen (**1**) or one nitrogen (**2** and **3**) from the pyrazole appended ligand occupied three coordination legs. The Ru-centroid distances were in the range of 1.656–1.687 Å, while the distances of Ru—Cl, Ru—N_{pz} and Ru—C bonds were in the range of 2.397–2.438, 2.090–2.108 and 2.179–2.217 Å respectively. These bond distances were comparable with previously reported Ru(II)(η^6-*p*-cymene) complexes [7,47,58,59,61,62]. A rare type of hydrogen bonding was seen between pyrazole NH and uncoordinated chloride with the bond distance of 3.016 Å in complex **1** [63]. In complex **3**, the thiophene moiety was disordered, which was successfully modeled with a ratio of 0.55:0.45 and there was no hydrogen bonding interaction between chloride (Cl1) and N—H when compared to previously reported complex of the same type [7].

3.3. Intercalative DNA binding study

In general, anticancer activity of complexes is related to their ability to bind with DNA through non-covalently or covalently [64]. The organometallic compounds of the type [Ru(arene)(en)] interacted specifically with N^7 in the guanine base pair of DNA. Additionally, the hydrophobic interaction between DNA and arene moiety was also observed [65]. The UV–Visible absorption titration is a useful technique to study the binding mode of DNA with compounds (Fig. 4) [66,67]. The Ru(II)(η^6-*p*-cymene) complexes showed a band around 265–272 nm which was assigned to intraligand transition. On titration of the Ru(II)(η^6-*p*-cymene) complexes with DNA, hypochromism (27.61–33.06%) was observed with a small red shift (1–2 nm), which indicated that the Ru(II)(η^6-*p*-cymene) complexes bound to CT-DNA through intercalation [68]. To determine the magnitude of binding affinity of the Ru(II)(η^6-*p*-cymene) complexes with CT-DNA, their K_b (binding constant) values were calculated using the Eq. [69], $[DNA]/(\varepsilon_a - \varepsilon_f) = [DNA]/(\varepsilon_b - \varepsilon_f) + 1/K_b(\varepsilon_b - \varepsilon_f)$ where [DNA] is the concentration of DNA in base pairs, ε_a is the apparent extinction coefficient value found by calculating A(observed)/[complex], ε_f is the extinction coefficient for the free compound, and ε_b is the extinction coefficient for the compound in the fully bound form. From the ratio of slope to intercept in the plot of $[DNA]/(\varepsilon_a - \varepsilon_f)$ *versus* [DNA] (Fig. 5), binding constant of the Ru(II)(η^6-*p*-cymene) complexes with DNA was calculated. The intrinsic binding constant (K_b) values were found to be 2.17 ($\pm$ 0.02) $\times 10^5$, 1.60 ($\pm$ 0.06) $\times 10^5$ and 1.79 ($\pm$ 0.03) $\times 10^5\,M^{-1}$ for complexes **1–3** respectively. Among the complexes, complex **1** with bidentate pyrazole ligand exhibited higher binding with DNA. The intrinsic binding constant (K_b) values of complexes **1–3** were comparable with those of similar ruthenium(II)-arene complexes reported previously [32,70,71].

3.4. Viscosity measurements

A classical intercalator lengthens DNA helix, which is due to the separation in the DNA base pairs when the compound slides in between and as a result of which the viscosity increases. In contrast, a partial, non-classical intercalation of molecules could bend (or kink) the DNA helix, reducing its length and, concomitantly, its viscosity. Complexes bind with DNA grooves cause less noticeable or no variation in the viscosity [72,73]. The viscosity of DNA increased with increasing the concentration of complexes **1–3** (0–60 μM) and the resultant graph is shown in Fig. 6. These results revealed binding of the complexes with DNA *via* intercalation. The ability of the complexes to increase the viscosity of DNA followed the order **1** > **3** > **2**.

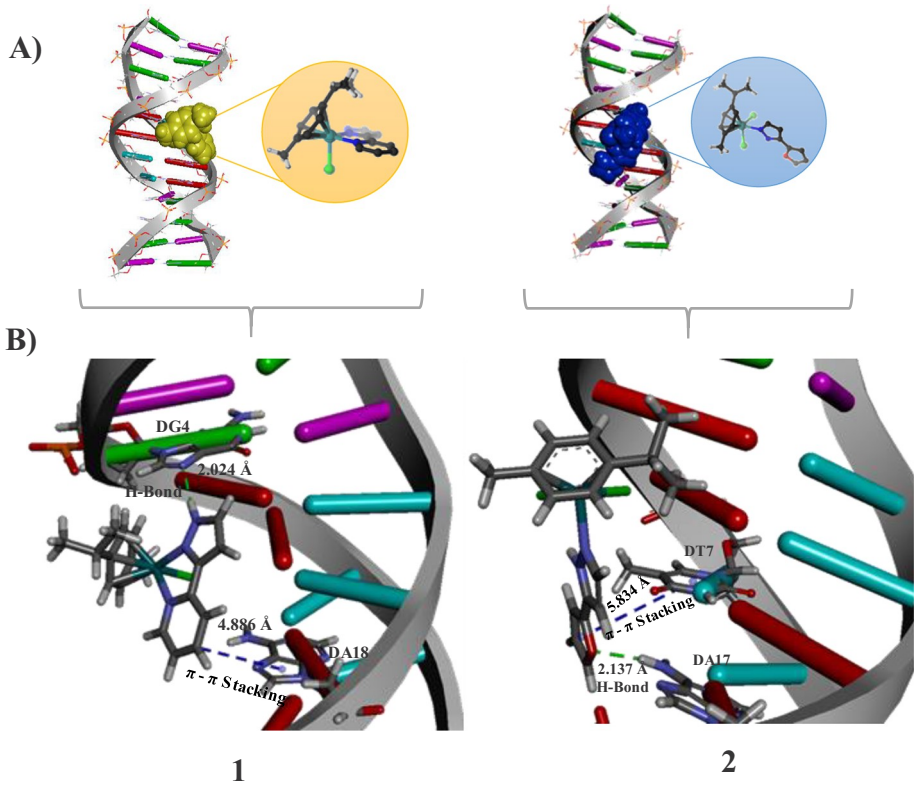

Fig. 8. A) Docked pose of the Ru(II)-*p*-cymene complexes (**1** and **2**) with B-DNA receptor shows intercalation [Indicated space-filling (CPK) model] mode of binding and optimized structures are given in the circles. B) Complex **1** shows crucial guanine N^7 position H-bond (green color) interaction. Complex **2**, interacts through pyrazole H-bond (green color line) and π-π stacking (blue color line) with adenine and thymine base pairs of receptor (B-DNA), respectively.

Table 2
Results of docking Glide score and Glide energy of B-DNA and topoisomerase I with complexes **1–8** obtained from Glide.

Complex	Glide score (kcal/mol)		Glide energy (kcal/mol)	
	B-DNA	Topoisomerase I	B-DNA	Topoisomerase I
1	−2.133	−2.446	−23.564	−25.367
2	−0.940	−0.381	−23.087	−30.351
3	−1.420	−1.215	−24.702	−28.019
4	−4.166	−3.316	−29.252	−28.977
5	−3.838	−2.160	−30.774	−29.331
6	−3.938	−3.214	−30.373	−28.755
7	−5.039	−3.277	−29.045	−33.502
8	−2.770	−3.015	−24.161	−32.256

3.5. Molecular docking studies

Complexes **1–3** might hydrolyse under physiological conditions to form their corresponding aqua complexes $[(\eta^6\text{-}p\text{-cymene})Ru(\eta^2\text{-}N,N\text{-L1})(OH_2)]^{2+}$ (**4**), $[(\eta^6\text{-}p\text{-cymene})Ru(\eta^1\text{-}N\text{-L2})(OH_2)Cl]^{+}$ (**5**), $[(\eta^6\text{-}p\text{-cymene})Ru(\eta^1\text{-}N\text{-L2})(OH_2)_2]^{2+}$ (**6**), $[(\eta^6\text{-}p\text{-cymene})Ru(\eta^1\text{-}N\text{-L3})(OH_2)Cl]^{+}$ (**7**), and $[(\eta^6\text{-}p\text{-cymene})Ru(\eta^1\text{-}N\text{-L3})(OH_2)_2]^{2+}$ (**8**) where chloride ligands were progressively replaced by water molecules. Therefore, the geometry of half-sandwich $Ru(\eta^6\text{-}p\text{-cymene})$ complexes **1–3** and their corresponding aqua complexes **4–8** was optimized at the DFT level and is presented in Fig. 7. DFT calculations confirmed pseudo-octahedral geometry of organoruthenium compounds. Table 1 shows that the experimental and computed bond parameters agree reasonably.

Molecular docking studies are very important to unravel the mechanism by which small molecules (ligand) bind with the active sites of large biomolecules [74,75]. The various interactions (van der Waals, hydrogen bonding, hydrophobic, charge transfer, and electrostatic) in ligand-receptor system that stabilize the complex can be understood from molecular docking study [76,77]. The binding efficiency of a biologically active drug is identified from its binding position and nature of interaction with receptor molecules. A scoring function to evaluate DNA/protein-ligand binding affinities had been used here and this is implemented in Glide 6.8 which is a competitive methodology for docking calculations. In the present work, molecular docking calculations were performed to understand the interactions of the pyrazole ligand based $Ru(II)(\eta^6\text{-}p\text{-cymene})$ complexes **1–8** with B-DNA whose sequence was dodecamer of $d(CGCGAATTCGCG)_2$ duplex structure (PDB ID: 1BNA). The most favorable docked poses are given in Fig. 8 and Figs. S13–S15, and the significant docked pose was picked out based on the highest Glide score and highest binding energy (Table 2). As it can be seen from Fig. 8A and Figs. S13A–S15A, the docked Ru(II) $(\eta^6\text{-}p\text{-cymene})$ complexes **1–8** could intercalate well into the B-DNA

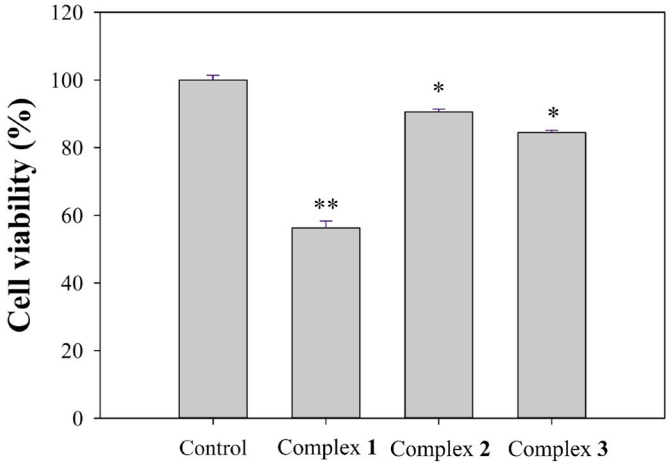

Fig. 9. The cytotoxic effect of complexes **1–3** (100 μM) on the cell viability of triple negative breast cancer MDA-MB-231 cells for 24 h. DMSO was used as a vehicle control group. Mean values ± SD from three independent experiment ($n = 3$) done in duplicate are presented. *$p < 0.05$, **$p < 0.01$.

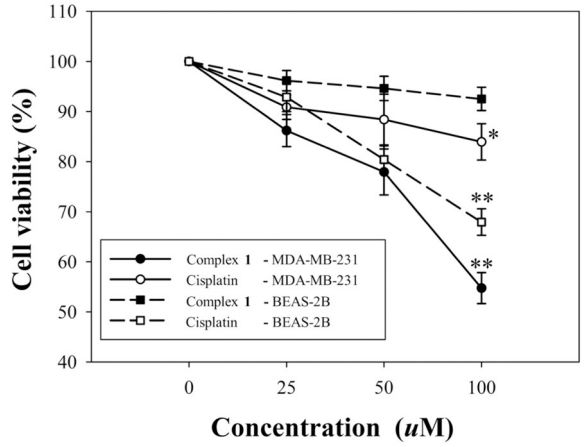

Fig. 10. The cell viability of MDA-MB-231 cancer cells and BEAS-2B normal cells after treatment with complex **1**, and cisplatin (0, 25, 50 and 100 μM) for 24 h. Mean values ± SD from three independent experiment ($n = 3$) done in duplicate are presented. *indicated $p < 0.05$ and ** indicated $p < 0.01$ *versus* control group.

receptor. In addition, the significant interactions are given in Fig. 8B and Figs. S13B–S15B. As it can be seen from Fig. 8B, interestingly, there was a crucial H-bonding (2.024 Å) interaction between guanine N^7 (DG4) and pyrazole ligand of **1**. Also, pyridine ring of the ligand interacted with adenine (DA18) base pairs of B-DNA, *via* π-π stacking (4.886 Å) interactions. The other complex **2** showed one H-bonding (2.137 Å) and π-π stacking (5.834 Å) interactions between the ligand, and adenine (DA17) and thymine (DT7) base pair, respectively. Fig. S13B clearly showed only one π-π stacking (5.833 Å) interaction between the ligand in complex **3** and adenine (DA18). Complex **4** interacted *via* two H-bonds (2.053 and 2.118 Å) with guanine (DG4 and DA5) base pairs and one π-sigma (2.672 Å) hydrophobic bond with adenine (DA5) base pair. In Fig. S14B, complexes **5** and **6** showed H-bonding interactions with various base pairs. Complex **5** was found to have three H-bonds (2.308, 2.706 and 2.351 Å) with adenine base pairs (DA5, DA6 and DT20). Complex **6** interacted through two H-bonds (2.019 and 2.134 Å) with the same guanine base pair (DG22). From Fig. S15B, it could be seen that complex **7** had four H-bonding (1.856, 2.674, 1.857 and 2.795 Å) interactions with two base pairs [guanine (DG4 and DG22) and adenine (DA5)] in the receptor binding pocket. Finally, complex **8** was found to have one H-bonding (1.768 Å) with guanine (DG4) and three π-π stacking interactions (4.919, 5.926 and 4.973 Å) with base pairs DG4 and DC3. The Glide scores (Table 2) show the strength of binding of the complexes as **7** (−5.039 kcal/mol) > **4** (−4.166 kcal/mol) > **6** (−3.938 kcal/mol) > **5** (−3.838 kcal/mol) > **8** (−2.770 kcal/mol) > **1** (−2.133 kcal/mol) > **3** (−1.420 kcal/mol) > **2** (−0.940 kcal/mol). Among the eight complexes, **7** exhibited stronger binding with B-DNA. The aqua complexes **4–8** of Ru(II)(η^6-*p*-cymene), that could be formed by hydrolysis of the original complexes in physiological conditions were more reactive than the original form of Ru(II)(η^6-*p*-cymene) complexes **1–3** and therefore they interacted more readily with nucleophilic active sites in biomolecules. When the binding strength of the original complexes **1–3** were compared, it followed the order **1** > **3** > **2** and this trend agreed very well with the experimental trend.

Similarly, molecular docking calculations were accomplished to know the interactions of Ru(II)(η^6-*p*-cymene) complexes **1–8** with topoisomerase I. The most favorable docked poses are given in Figs. S16–S19. The significant docked poses were picked out based on the highest Glide score and highest binding energy (Table 2). Figs. S16A–S19A revealed that the Ru(II)(η^6-*p*-cymene) complexes bound through intercalation (**1**), minor (**2**, **4**, **5** and **6**), and major (**3**, **7** and **8**) grooves mode with topoisomerase receptor. In addition, the significant non-covalent interactions between the ligand and receptor are given in Figs. S16B–S19B. It can be seen from Fig. S16B that the pyrazole ligand in complex **1** had significant H-bonding (2.154 Å) interaction with thymine base (DT108) pair and one π-alkyl hydrophobic interaction with amino acid residue (ALA635) in receptor binding pocket. In the same way, complex **2** showed one H-bonding (2.043 Å) interaction with glycine amino acid residue (GLA704) and one π-alkyl (5.258 Å) hydrophobic interaction with arginine amino acid (ARG258) in the receptor pocket. Fig. S17B revealed that complex **3** had one H-bond (2.510 Å) with thymine base pair (DT106) and one π-alkyl (4.973 Å) hydrophobic interaction with arginine amino acid (ARG708), and complex **4** bridged through two H-bonds (1.590 and 2.634 Å) with thymine base pairs (DT106 and DT107). Fig. S18B showed that complex **5** had three H-bonds (2.513, 2.724 and 1.989 Å) with thymine base pairs (DT106 and DT107) and one amino acid residue (GLN704), respectively, and complex **6** had mainly two H-bonds (1.927 and 2.514 Å) with glycine amino acid (GLN704) and thymine base pair (DT106), respectively. In addition, it had one π-alkyl (5.449 Å) hydrophobic interaction and π-cation (4.031 Å) electrostatic interaction with arginine amino acid (ARG708). Finally, from Fig. S19B, it could be seen that complex **7** had one H-bonding (1.998 Å) interaction and one π-sigma (3.716 Å) hydrophobic interaction with thymine base pair (DT107) and isoleucine amino acid (ILE616), respectively. Complex **8** had two H-bonds (2.487 and 2.744 Å) with asparagine (ASN620 and ASN707) amino acid residues. The calculated Glide score (Table 2) showed the binding strength of the complexes in the order, **4** (−3.316 kcal/mol) > **7** (−3.277 kcal/mol) > **6** (−3.214 kcal/mol) > **8** (−3.015 kcal/mol) > **1** (−2.446 kcal/mol) > **5** (−2.160 kcal/mol) > **3** (−1.215 kcal/mol) > **2** (−0.381 kcal/mol). Among the complexes **1–8**, complex **4** displayed a stronger interaction with topoisomerase I, aqua complexes were strongly binding than the original complexes, and the order of binding strength among the original complexes (**1** > **3** > **2**) agreed excellently with the experimental trend.

3.6. In vitro cytotoxicity

Cytotoxicity of Ru(II)(η^6-*p*-cymene) complexes **1–3** was tested

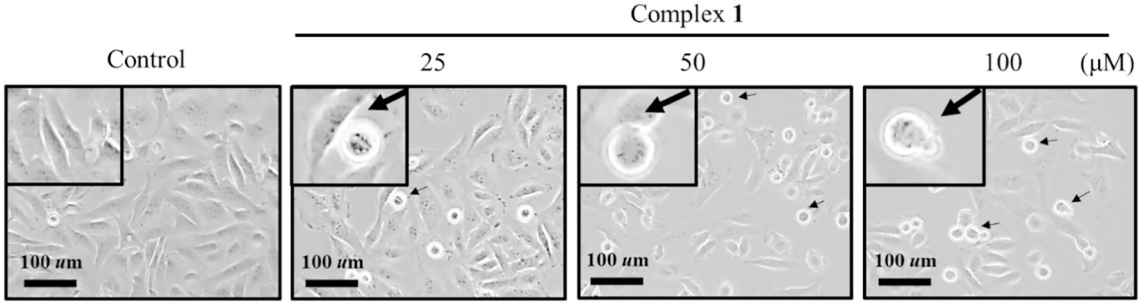

Fig. 11. The morphological changes of triple negative breast cancer MDA-MB-231 cells treated with (0–100 μM) complex **1** for 24 h. The black arrows indicated the shrinkage and rounding of cells compared to the control group.

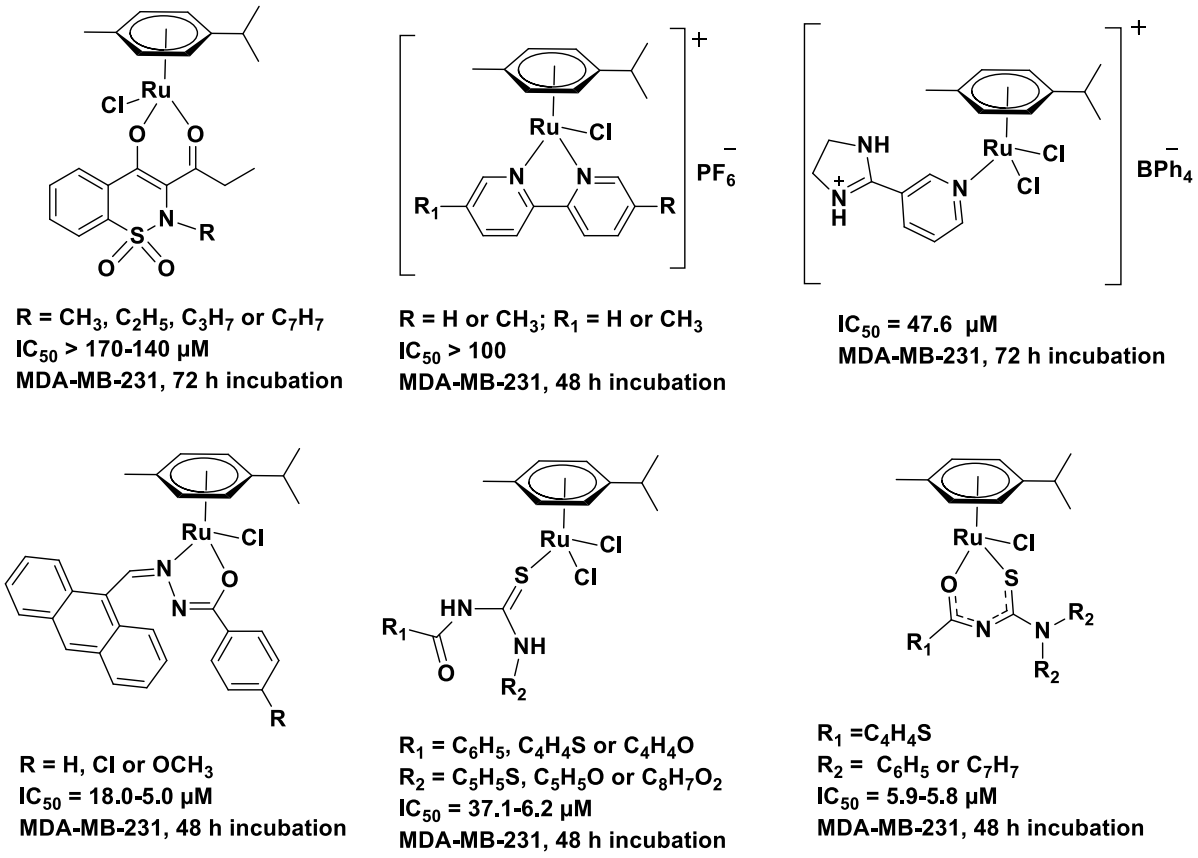

Fig. 12. IC_{50} values of reported [[RuCl(η^6-*p*-cymene)L]/[$RuCl_2$(η^6-*p*-cymene)L] type complexes (L is a bidentate/monodentate ligand).

against TNBC MDA-MB-231 cells by MTS assay for 24 h at 100 μM concentration. The results of percentage cell viability are displayed in Fig. 9. Complexes **2** and **3** showed only slight cytotoxic effect on TNBC MDA-MB-231 breast cancer cells with the cell viability of 90.6 and 84.5%, respectively. However, complex **1** with bidentate ligand showed the highest inhibitory activity with the cell viability of 56.3%. Therefore, complex **1** with different concentrations (0, 25, 50, and 100 μM) was screened in the same cell line along with cisplatin [78]. As shown in Fig. 10, the cell viability on MDA-MB-231 cancer cells for 24 h of cisplatin was 89.1 (25 μM), 86.4 (50 μM), and 83.9 (100 μM) %. However, complex **1** displayed the cell viability of 86.2 (25 μM), 77.9 (50 μM), and 54.7 (100 μM) %, which indicated that the bioactivity of complex **1** was higher than that of cisplatin. Moreover, the cell viability on BEAS-2B normal cells for 24 h of cisplatin (25, 50, and 100 μM) was 96.2, 80.4 and 67.9%, respectively. The cell viability of complex **1** (25, 50, and 100 μM) on BEAS-2B normal cells for 24 h was 96.2, 94.6, and 92.5%, respectively. These results indicated that complex **1** exerted a selective cytotoxic activity against breast cancer cells. Likewise, the morphological changes including number reduction, shrinkage and rounding of cells, which are hallmarks of apoptosis were observed in MDA-MB-231 cells following the treatment with complex **1** (25, 50, and 100 μM) for 24 h (Fig. 11). The cytotoxicity of the complexes followed the order **1** > cisplatin > **2** ≈ **3**, and complex **1** induced significant changes in cellular morphology, which account for high activity of **1**. The IC_{50} value for complex **1** against MBA-MB-231 human breast cancer cell line was around 110 μM. The present complexes notably **1** exhibited good activity than previously reported Ru-*p*-cymene complexes [79,80], but less activity than ruthenium-*p*-cymene complexes containing thiourea/hydrozone ligands [81–83]. The cytotoxicity of [RuCl(η^6-*p*-cymene)L]/[$RuCl_2$(η^6-*p*-cymene)L] type complexes (L is a bidentate/monodentate ligand) is summarized in Fig. 12. It is evident from the comparison that the present complexes displayed comparable activity with known Ru-*p*-cymene complexes (Fig. 11). Even though the complexes showed higher IC_{50} values, this is not necessarily a negative property for an anticancer drug candidate. The mechanisms of action of Ru compounds are still not fully understood. NAMI-A and RAPTA compounds which have low activity *in vitro*, show high activity against metastases *in vivo*, demonstrate that high IC_{50} value might not be an appropriate reason to discard a compound from further development [84–87].

4. Conclusions

Mono- and bi-dentate Ru(II)-*p*-cymene complexes were synthesized and characterized by elemental analyses, and various spectroscopic techniques like FT-IR, UV–Visible, NMR, and mass. The solid-state structures of all the complexes were confirmed by single crystal X-ray diffraction technique; it is clearly understood that the complexes adopted piano stool geometry around Ru(II) ion. All the complexes efficiently bound with DNA through intercalation and followed the order **1** > **3** > **2** agreeing with experimental results. Complexes **1–3** could form aqua complexes **4–8** upon hydration under physiological conditions and docking calculations revealed that aqua complexes **4–8** strongly bound than original complexes **1–3**. Calculations showed that complex **1** had a crucial H-bonding interaction with guanine N^7 *via* pyrazole ligand. Similarly, with topoisomerase I, aqua complexes bound strongly than original complexes and among the original complexes the order of binding was **1** > **3** > **2**. Contrastingly, here, **1** bound through intercalation while the other two preferred groove binding modes. Further analysis of non-covalent interactions showed that complex **1** - topoisomerase I system was strongly stabilized by one strong H-bonding interaction and one π-alkyl hydrophobic interaction. Triple negative breast cancer (TNBC) cells do not express estrogen receptor, HER2 and progesterone receptor and therefore lack efficacy for targeting these

above proteins [88], resulting in the poor prognosis of breast cancer patients. *In vitro* cytotoxicity results revealed that complex **1** (with bidentate ligand) exhibited more activity against MDA-MB-231 cells than complexes **2**, **3**, and cisplatin, which may be attributed to the presence hydrogen bond between the ligand and biomolecule. Furthermore, TNBC has shown resistance to clinical anticancer drugs including cisplatin [89]. In this study, our results showed that complex **1** exerted a selective cytotoxic activity against TNBC MDA-MB-231. Accordingly, our present work suggests the selective anticancer potential of the Ru (II)-*p*-cymene complexes towards TNBC, which deserves further investigation in the future.

Acknowledgments

The authors thank all the reviewers for their critical and helpful comments. We gratefully acknowledge financial support from the Ministry of Science and Technology, Taiwan (MOST107-2113-M-037-004), NSYSU-KMU Joint Research Project (NSYSUKMU 107-P003), and Taiwan Experience Education Program (TEEP) of Ministry of Education, Taiwan. J. H. thanks the University Grants Commission for the fellowship (F1-17.1/2012-13/RGNF-2012-13-ST-AND-18716). P.V. and G.S. thank the Council of Scientific and Industrial Research (CSIR) for the award of an Emeritus Scientistship (Ref. No. 21(0936)/12/EMR–II), and DST-PURSE HPC Facility (SR/FT/LS-113/2009) of Bharathidasan University. We also thank for Prof. Ming-Hon Hou, director, Institute of Genomics and Bioinformatics, National Chung Hsing University for the research facilities and space provided about re-perform cell associated experiments.

Appendix A. Supplementay data

References

[1] G.H. Christian, D.P. Andrew, A.N. Alexey, Curr. Top. Med. Chem. 11 (2011) 2688–2702.
[2] N. Chavain, C. Biot, Curr. Med. Chem. 17 (2010) 2729–2745.
[3] G. Gasser, I. Ott, N. Metzler-Nolte, J. Med. Chem. 54 (2011) 3–25.
[4] E. Meggers, Chem. Commun. (2009) 1001–1010.
[5] D.-L. Ma, D.S.-H. Chan, C.-H. Leung, Acc. Chem. Res. 47 (2014) 3614–3631.
[6] P. Chène, Nat. Rev. Drug Discov. 1 (2002) 665.
[7] A. Basava Punna Rao, K. Gulati, N. Joshi, D.K. Deb, D. Rambabu, W. Kaminsky, K.M. Poluri, M.R. Kollipara, Inorg. Chim. Acta 462 (2017) 223–235.
[8] C.S. Slone, D.A. Weinberger, C.A. Mirkin, Prog. Inorg. Chem. (2007) 233–350.
[9] B. Therrien, T.R. Ward, Angew. Chem. Int. Ed. 38 (1999) 405–408.
[10] P. Crochet, M.A. Fernández-Zumel, C. Beauquis, J. Gimeno, Inorg. Chim. Acta 356 (2003) 114–120.
[11] K.Y. Ghebreyessus, J.H. Nelson, J. Organomet. Chem. 669 (2003) 48–56.
[12] V. Ritleng, P. Bertani, M. Pfeffer, C. Sirlin, J. Hirschinger, Inorg. Chem. 40 (2001) 5117–5122.
[13] C.A. Merlic, M.E. Pauly, J. Am. Chem. Soc. 118 (1996) 11319–11320.
[14] Z. Kabouche, C. Bruneau, P.H. Dixneuf, Tetrahedron Lett. 32 (1991) 5359–5362.
[15] K. Philippot, D. Devanne, P.H. Dixneuf, J. Chem. Soc. Chem. Commun. (1990) 1199–1200.
[16] H. Nagashima, H. Kondo, T. Hayashida, Y. Yamaguchi, M. Gondo, S. Masuda, K. Miyazaki, K. Matsubara, K. Kirchner, Coord. Chem. Rev. 245 (2003) 177–190.
[17] R.E. Aird, J. Cummings, A.A. Ritchie, M. Muir, R.E. Morris, H. Chen, P.J. Sadler, D.I. Jodrell, Br. J. Cancer 86 (2002) 1652.
[18] L.A. Huxham, E.L.S. Cheu, B.O. Patrick, B.R. James, Inorg. Chim. Acta 352 (2003) 238–246.
[19] S. Leijen, S.A. Burgers, P. Baas, D. Pluim, M. Tibben, E. van Werkhoven, E. Alessio, G. Sava, J.H. Beijnen, J.H.M. Schellens, Investig. New Drugs 33 (2015) 201–214.
[20] Y.K. Yan, M. Melchart, A. Habtemariam, P.J. Sadler, Chem. Commun. (2005) 4764–4776.
[21] L.K. Filak, G. Mühlgassner, F. Bacher, A. Roller, M. Galanski, M.A. Jakupec, B.K. Keppler, V.B. Arion, Organometallics 30 (2011) 273–283.
[22] S.M. Meier, M. Novak, W. Kandioller, M.A. Jakupec, V.B. Arion, N. Metzler-Nolte, B.K. Keppler, C.G. Hartinger, Chem. Eur. J. 19 (2013) 9297–9307.
[23] M. Carcelli, A. Bacchi, P. Pelagatti, G. Rispoli, D. Rogolino, T.W. Sanchez, M. Sechi, N. Neamati, J. Inorg. Biochem. 118 (2013) 74–82.
[24] T. Küster, N. Lense, F. Barna, A. Hemphill, M.K. Kindermann, J.W. Heinicke, C.A. Vock, J. Med. Chem. 55 (2012) 4178–4188.
[25] M. Adams, Y. Li, H. Khot, C. De Kock, P.J. Smith, K. Land, K. Chibale, G.S. Smith, Dalton Trans. 42 (2013) 4677–4685.
[26] A. Martínez, T. Carreon, E. Iniguez, A. Anzellotti, A. Sánchez, M. Tyan, A. Sattler, L. Herrera, R.A. Maldonado, R.A. Sánchez-Delgado, J. Med. Chem. 55 (2012) 3867–3877.
[27] R. Schuecker, R.O. John, M.A. Jakupec, V.B. Arion, B.K. Keppler, Organometallics 27 (2008) 6587–6595.
[28] M. Schmidlehner, P.-S. Kuhn, C.M. Hackl, A. Roller, W. Kandioller, B.K. Keppler, J. Organomet. Chem. 772-773 (2014) 93–99.
[29] R.E. Morris, R.E. Aird, P. del Socorro Murdoch, H. Chen, J. Cummings, N.D. Hughes, S. Parsons, A. Parkin, G. Boyd, D.I. Jodrell, P.J. Sadler, J. Med. Chem. 44 (2001) 3616–3621.
[30] K. Purkait, S. Karmakar, S. Bhattacharyya, S. Chatterjee, S.K. Dey, A. Mukherjee, Dalton Trans. 44 (2015) 5969–5973.
[31] S. Bhattacharyya, K. Purkait, A. Mukherjee, Dalton Trans. 46 (2017) 8539–8554.
[32] R.A. Khan, F. Arjmand, S. Tabassum, M. Monari, F. Marchetti, C. Pettinari, J. Organomet. Chem. 771 (2014) 47–58.
[33] M. Gras, B. Therrien, G. Süss-Fink, A. Casini, F. Edafe, P.J. Dyson, J. Organomet. Chem. 695 (2010) 1119–1125.
[34] E.C. Constable, P.J. Steel, Coord. Chem. Rev. 93 (1989) 205–223.
[35] H. Ohki, K. Hirotani, H. Naito, S. Ohsuki, M. Minami, A. Ejima, Y. Koiso, Y. Hashimoto, Bioorg. Med. Chem. Lett. 12 (2002) 3191–3193.
[36] H. Naito, S. Ohsuki, M. Sugimori, R. Atsumi, M. Minami, Y. Nakamura, M. Ishii, K. Hirotani, E. Kumazawa, A. Ejima, Chem. Pharm. Bull. 50 (2002) 453–462.
[37] J.K. Barton, A. Danishefsky, J. Goldberg, J. Am. Chem. Soc. 106 (1984) 2172–2176.
[38] C. Hiort, P. Lincoln, B. Norden, J. Am. Chem. Soc. 115 (1993) 3448–3454.
[39] S. Campagna, G. Denti, G. De Rosa, L. Sabatino, M. Ciano, V. Balzani, Inorg. Chem. 28 (1989) 2565–2570.
[40] K. Bierig, R.J. Morgan, S. Tysoe, H.D. Gafney, T.C. Strekas, A.D. Baker, Inorg. Chem. 30 (1991) 4898–4903.
[41] M.A. Bennett, T.N. Huang, T.W. Matheson, A.K. Smith, S. Ittel, W. Nickerson, Inorg. Synth. (2007) 74–78.
[42] Y.-i. Lin, S.A. Lang, J. Heterocyclic Chem. 14 (1977) 345–347.
[43] M.A. Halcrow, E.J.L. McInnes, F.E. Mabbs, I.J. Scowen, M. McPartlin, H.R. Powell, J.E. Davies, J. Chem. Soc. Dalton Trans. (1997) 4025–4036.
[44] J.C. Calabrese, P.J. Domaille, S. Trofimenko, G.J. Long, Inorg. Chem. 30 (1991) 2795–2801.
[45] G. M. Sheldrick, in, University of Gottingen, Gottingen, Germany., 2014.
[46] N. Selvakumaran, L. Sandhiya, N.S.P. Bhuvanesh, K. Senthilkumar, R. Karvembu, New J. Chem. 40 (2016) 5401–5413.
[47] K. Jeyalakshmi, J. Haribabu, C. Balachandran, N.S.P. Bhuvanesh, N. Emi, R. Karvembu, New J. Chem. 41 (2017) 2672–2686.
[48] K.N.A. Rahman, J. Haribabu, C. Balachandran, N.S.P. Bhuvanesh, R. Karvembu, A. Sreekanth, Polyhedron 135 (2017) 26–35.
[49] C. Lee, W. Yang, R.G. Parr, Phys. Rev. B 37 (1988) 785–789.
[50] A.D. Becke, J. Chem. Phys. 98 (1993) 5648–5652.
[51] M.J. Frisch, G.W. Trucks, H.B. Schlegel, G.E. Scuseria, M.A. Robb, J.R. Cheeseman, G. Scalmani, V. Barone, B. Mennucci, G.A. Petersson, H. Nakatsuji, M. Caricato, X. Li, H.P. Hratchian, A.F. Izmaylov, J. Bloino, G. Zheng, J.L. Sonnenberg, M. Hada, M. Ehara, K. Toyota, R. Fukuda, J. Hasegawa, M. Ishida, T. Nakajima, Y. Honda, O. Kitao, H. Nakai, T. Vreven, J.A. Montgomery Jr., J.E. Peralta, F. Ogliaro, M. Bearpark, J.J. Heyd, E. Brothers, K.N. Kudin, V.N. Staroverov, R. Kobayashi, J. Normand, K. Raghavachari, A. Rendell, J.C. Burant, S.S. Iyengar, J. Tomasi, M. Cossi, N. Rega, J.M. Millam, M. Klene, J.E. Knox, J.B. Cross, V. Bakken, C. Adamo, J. Jaramillo, R. Gomperts, R.E. Stratmann, O. Yazyev, A.J. Austin, R. Cammi, C. Pomelli, J.W. Ochterski, R.L. Martin, K. Morokuma, V.G. Zakrzewski, G.A. Voth, P. Salvador, J.J. Dannenberg, S. Dapprich, A.D. Daniels, O. Farkas, J.B. Foresman, J.V. Ortiz, J. Cioslowski, D.J. Fox, Gaussian 09, Revision D.01, Gaussian, Inc., Wallingford, CT, 2009.
[52] J. Millam, GaussView, version 5, Semichem Inc., Shawnee Mission, KS, 2009.
[53] T.A. Halgren, R.B. Murphy, R.A. Friesner, H.S. Beard, L.L. Frye, W.T. Pollard, J.L. Banks, J. Med. Chem. 47 (2004) 1750–1759.
[54] R.A. Friesner, R.B. Murphy, M.P. Repasky, L.L. Frye, J.R. Greenwood, T.A. Halgren, P.C. Sanschagrin, D.T. Mainz, J. Med. Chem. 49 (2006) 6177–6196.
[55] K.S. Watts, P. Dalal, R.B. Murphy, W. Sherman, R.A. Friesner, J.C. Shelley, J. Chem. Inf. Model. 50 (2010) 534–546.
[56] W.L. DeLano, The PyMOL Molecular Graphics System (2002), DeLano Scientific, Palo Alto, CA, USA, 2002http://www.pymol.org.
[57] W.-T. Chang, W. Liu, Y.-H. Chiu, B.-H. Chen, S.-C. Chuang, Y.-C. Chen, Y.-T. Hsu, M.-J. Lu, S.-J. Chiou, C.-K. Chou, C.-C. Chiu, Molecules 22 (2017) 854.
[58] M.M. Sheeba, M. Muthu Tamizh, L.J. Farrugia, A. Endo, R. Karvembu, Organometallics 33 (2014) 540–550.
[59] W. Su, Z. Tang, P. Li, G. Wang, Q. Xiao, Y. Li, S. Huang, Y. Gu, Z. Lai, Y. Zhang, Dalton Trans. 45 (2016) 19329–19340.
[60] J. Palmucci, F. Marchetti, R. Pettinari, C. Pettinari, R. Scopelliti, T. Riedel, B. Therrien, A. Galindo, P.J. Dyson, Inorg. Chem. 55 (2016) 11770–11781.
[61] K. Jeyalakshmi, J. Haribabu, N.S.P. Bhuvanesh, R. Karvembu, Dalton Trans. 45 (2016) 12518–12531.
[62] K. Purkait, S. Chatterjee, S. Karmakar, A. Mukherjee, Dalton Trans. 45 (2016) 8541–8555.
[63] J. Haribabu, D.S. Ranade, N.S.P. Bhuvanesh, P.P. Kulkarni, R. Karvembu, ChemistrySelect 2 (2017) 11638–11644.
[64] V. Brabec, O. Nováková, Drug Resist. Updat. 9 (2006) 111–122.
[65] O. Novakova, H. Chen, O. Vrana, A. Rodger, P.J. Sadler, V. Brabec, Biochemistry 42 (2003) 11544–11554.
[66] J.M. Kelly, A.B. Tossi, D.J. McConnell, C. OhUigin, Nucleic Acids Res. 13 (1985) 6017–6034.
[67] S.A. Tysoe, R.J. Morgan, A.D. Baker, T.C. Strekas, J. Phys. Chem. 97 (1993) 1707–1711.

[68] E. Ramachandran, V. Gandin, R. Bertani, P. Sgarbossa, K. Natarajan, N.S.P. Bhuvanesh, A. Venzo, A. Zoleo, A. Glisenti, A. Dolmella, A. Albinati, C. Marzano, J. Inorg. Biochem. 182 (2018) 18–28.
[69] M. Alagesan, N.S.P. Bhuvanesh, N. Dharmaraj, Eur. J. Med. Chem. 78 (2014) 281–293.
[70] R.K. Gupta, R. Pandey, G. Sharma, R. Prasad, B. Koch, S. Srikrishna, P.-Z. Li, Q. Xu, D.S. Pandey, Inorg. Chem. 52 (2013) 3687–3698.
[71] J. Haribabu, G. Sabapathi, M.M. Tamizh, C. Balachandran, N.S.P. Bhuvanesh, P. Venuvanalingam, R. Karvembu, Organometallics 37 (2018) 1242–1257.
[72] S. Ramakrishnan, M. Palaniandavar, Dalton Trans. (2008) 3866–3878.
[73] N. Selvakumaran, N.S.P. Bhuvanesh, R. Karvembu, Dalton Trans. 43 (2014) 16395–16410.
[74] J. Lakshmipraba, S. Arunachalam, R.V. Solomon, P. Venuvanalingam, A. Riyasdeen, R. Dhivya, M.A. Akbarsha, J. Biomol. Struct. Dyn. 33 (2015) 877–891.
[75] S. Veeralakshmi, G. Sabapathi, S. Nehru, P. Venuvanalingam, S. Arunachalam, Colloids Surf. B. Biointerfaces 153 (2017) 85–94.
[76] K. Nagaraj, G. Velmurugan, S. Sakthinathan, P. Venuvanalingam, S. Arunachalam, Dalton Trans. 43 (2014) 18074–18086.
[77] S. Veeralakshmi, S. Nehru, G. Sabapathi, S. Arunachalam, P. Venuvanalingam, P. Kumar, C. Anusha, V. Ravikumar, RSC Adv. 5 (2015) 31746–31758.
[78] R. Czarnomysy, A. Surażyński, B. Popławska, E. Rysiak, N. Pawłowska, A. Czajkowska, K. Bielawski, A. Bielawska, Mol. Cell. Biochem. 427 (2017) 13–22.
[79] F. Aman, M. Hanif, W.A. Siddiqui, A. Ashraf, L.K. Filak, J. Reynisson, T. Söhnel, S.M.F. Jamieson, C.G. Hartinger, Organometallics 33 (2014) 5546–5553.
[80] L. Colina-Vegas, W. Villarreal, M. Navarro, C.R. de Oliveira, A.E. Graminha, P.I.d.S. Maia, V.M. Deflon, A.G. Ferreira, M.R. Cominetti, A.A. Batista, J. Inorg. Biochem. 153 (2015) 150–161.
[81] S. Nikolić, D.M. Opsenica, V. Filipović, B. Dojčinović, S. Aranđelović, S. Radulović, S. Grgurić-Šipka, Organometallics 34 (2015) 3464–3473.
[82] M.K.M. Subarkhan, R. Ramesh, Inorg. Chem. Front. 3 (2016) 1245–1255.
[83] L. Colina-Vegas, L. Luna-Dulcey, A.M. Plutín, E.E. Castellano, M.R. Cominetti, A.A. Batista, Dalton Trans. 46 (2017) 12865–12875.
[84] G. Sava, I. Capozzi, K. Clerici, G. Gagliardi, E. Alessio, G. Mestroni, Clin. Exp. Metastasis 16 (1998) 371–379.
[85] G. Sava, R. Gagliardi, M. Cocchietto, K. Clerici, I. Capozzi, M. Marrella, E. Alessio, G. Mestroni, R. Milanino, Pathol. Oncol. Res. 4 (1998) 30–36.
[86] J.M. Rademaker-Lakhai, D. van den Bongard, D. Pluim, J.H. Beijnen, J.H.M. Schellens, Clin. Cancer Res. 10 (2004) 3717–3727.
[87] C. Scolaro, A. Bergamo, L. Brescacin, R. Delfino, M. Cocchietto, G. Laurenczy, T.J. Geldbach, G. Sava, P.J. Dyson, J. Med. Chem. 48 (2005) 4161–4171.
[88] E.A. Rakha, M.E. El-Sayed, A.R. Green, A.H.S. Lee, J.F. Robertson, I.O. Ellis, Cancer 109 (2007) 25–32.
[89] J. Xu, T. Sun, X. Guo, Y. Wang, M. Jing, Oncol. Lett. 15 (2018) 2855–2862.